Supporting Information

Discovering the Importance of $ClO^{\bullet}$ in a Coupled Electrochemical System for the Simultaneous Removal of Carbon and Nitrogen from Secondary Coking Wastewater Effluent

Wenxiao Zheng,[†] Liuyi Zhu,[†] Sheng Liang,[†] Jinshao Ye,[‡] Xin Yang,[§] Zhenchao Lei,[†] Zhang Yan,[†] Yongdong Li,[†] Chaohai Wei,[†] and Chunhua Feng[*,†]

[†] The Key Lab of Pollution Control and Ecosystem Restoration in Industry Clusters, Ministry of Education, School of Environment and Energy, South China University of Technology, Guangzhou 510006, PR China

[‡] Guangdong Key Laboratory of Environmental Pollution and Health, School of Environment, Jinan University, Guangzhou 510632, PR China

[§] School of Environmental Science and Engineering, Sun Yat-sen University, Guangzhou 510275, PR China

Contents **Page**

Text S1. Electron Paramagnetic Resonance Measurements (EPR) for Identifying Active Species. For EPR measurements, 1 mL of the sample after 1 minute of electrolysis was immediately mixed with 10 μL DMPO. Then, the EPR spectra were obtained on a Bruker EMX A300-10/12 (Germany) within 5 min. The measurements were conducted using a radiation of 9.85 GHz (X band) with a center field of 3510 G, a modulation frequency of 100 kHz, a sweep width of 100 G, a sweep time of 40.01 s, a time constant of 0.01 ms, and a microwave power of 20.00 mW at room temperature.

Text S2. Determination of the Steady-State Concentrations of $HO^{\bullet}$, $Cl^{\bullet}$, $Cl_2^{\bullet-}$, and $ClO^{\bullet}$ by Probe Experiments. The steady-state concentrations of $HO^{\bullet}$, $Cl^{\bullet}$, $Cl_2^{\bullet-}$, and $ClO^{\bullet}$ in different wastewater systems were measured using nitrobenzene (NB), benzoic acid (BA), 1,4-dimethoxybenzene (DMOB), and carbamazepine (CBZ) (each with an initial concentration of 50 μM) as the probe compounds. They were carefully selected based on the facts that NB can only react with $HO^{\bullet}$ ($k_{HO\bullet, NB} = 3.9 \times 10^9$ M^{-1} s^{-1});[1] BA can be oxidized by both $HO^{\bullet}$ ($k_{HO\bullet, BA} = 5.9 \times 10^9$ M^{-1} s^{-1}) and $Cl^{\bullet}$ ($k_{Cl\bullet, BA} = 1.8 \times 10^{10}$ M^{-1} s^{-1});[2,3] DMOB reacts with $HO^{\bullet}$, $Cl^{\bullet}$, and $ClO^{\bullet}$ at appreciably high rates ($k_{HO\bullet, DMOB} = 7.0 \times 10^9$ M^{-1} s^{-1}, $k_{Cl\bullet, DMOB} = 1.8 \times 10^{10}$ M^{-1} s^{-1}, and $k_{ClO\bullet, DMOB} = 2.1 \times 10^9$ M^{-1} s^{-1});[4,5] and CBZ can be degraded by all the radicals ($k_{HO\bullet, CBZ} = 8.8 \times 10^9$ M^{-1} s^{-1}, $k_{Cl\bullet, CBZ} = 3.3 \times 10^{10}$ M^{-1} s^{-1}, $k_{ClO\bullet, CBZ} = 1.97 \times 10^8$ M^{-1} s^{-1}, and $k_{Cl_2\bullet-, CBZ} = 4.3 \times 10^7$ M^{-1} s^{-1}).[6-8] It should be noted that four probes, including NB, BA, DMOB, and CBZ were simultaneously added to the coupled electrochemical system that was fed with the real wastewater. The degradation kinetics of NB, BA, DMOB, and CBZ in the electrochemical system can be expressed as eqs S1−S4. Through integration, the relationships between the apparent rate constants and the steady-state concentrations of radicals ("steady state" is abbreviated as "ss") were established (eqs S5−S8). Then, the concentrations of $HO^{\bullet}$, $Cl^{\bullet}$, $Cl_2^{\bullet-}$, and $ClO^{\bullet}$ could be quantified by iteration (eqs S9−S12).

$$\frac{d[NB]}{dt} = -k_{NB, HO\bullet}[HO^{\bullet}]_{ss}[NB] \tag{S1}$$

$$\frac{d[BA]}{dt} = -(k_{BA, HO\bullet}[HO^{\bullet}]_{ss} + k_{BA, Cl\bullet}[Cl^{\bullet}]_{ss})[BA] \tag{S2}$$

$$\frac{d[DMOB]}{dt} = -(k_{DMOB, HO\bullet}[HO^{\bullet}]_{ss} + k_{DMOB, Cl\bullet}[Cl^{\bullet}]_{ss} + k_{DMOB, ClO\bullet}[ClO^{\bullet}]_{ss})[DMOB] \tag{S3}$$

$$\frac{d[CBZ]}{dt} = -(k_{CBZ, HO\bullet}[HO^{\bullet}]_{ss} + k_{CBZ, Cl\bullet}[Cl^{\bullet}]_{ss} + k_{CBZ, ClO\bullet}[ClO^{\bullet}]_{ss}$$

$$+k_{\mathrm{CBZ,\ Cl_2^{\bullet-}}}[\mathrm{Cl_2^{\bullet-}}]_{ss})[\mathrm{CBZ}] \tag{S4}$$

Integrating eqs S1−S4 can yield:

$$\ln\frac{[\mathrm{NB}]}{[\mathrm{NB}]_0} = -k_{\mathrm{NB,\ HO^\bullet}}[\mathrm{HO^\bullet}]_{ss}t = -k_{\mathrm{NB}}t \tag{S5}$$

$$\ln\frac{[\mathrm{BA}]}{[\mathrm{BA}]_0} = -(k_{\mathrm{BA,\ HO^\bullet}}[\mathrm{HO^\bullet}]_{ss} + k_{\mathrm{BA,\ Cl^\bullet}}[\mathrm{Cl^\bullet}]_{ss})t = -k_{\mathrm{BA}}t \tag{S6}$$

$$\ln\frac{[\mathrm{DMOB}]}{[\mathrm{DMOB}]_0} = -(k_{\mathrm{DMOB,\ HO^\bullet}}[\mathrm{HO^\bullet}]_{ss} + k_{\mathrm{DMOB,\ Cl^\bullet}}[\mathrm{Cl^\bullet}]_{ss} + k_{\mathrm{DMOB,\ ClO^\bullet}}[\mathrm{ClO^\bullet}]_{ss})t$$

$$= -k_{\mathrm{DMOB}}t \tag{S7}$$

$$\ln\frac{[\mathrm{CBZ}]}{[\mathrm{CBZ}]_0} = -(k_{\mathrm{CBZ,\ HO^\bullet}}[\mathrm{HO^\bullet}]_{ss} + k_{\mathrm{CBZ,\ Cl^\bullet}}[\mathrm{Cl^\bullet}]_{ss} + k_{\mathrm{CBZ,\ ClO^\bullet}}[\mathrm{ClO^\bullet}]_{ss}$$

$$+ k_{\mathrm{CBZ,\ Cl_2^{\bullet-}}}[\mathrm{Cl_2^{\bullet-}}]_{ss})t$$

$$= -k_{\mathrm{CBZ}}t \tag{S8}$$

Therefore, $[\mathrm{HO^\bullet}]_{ss}$, $[\mathrm{Cl^\bullet}]_{ss}$, $[\mathrm{ClO^\bullet}]_{ss}$ and $[\mathrm{Cl_2^{\bullet-}}]_{ss}$ can be quantified as follows：

$$[\mathrm{HO^\bullet}]_{ss} = \frac{k_{\mathrm{NB}}}{k_{\mathrm{NB,\ HO^\bullet}}} \tag{S9}$$

$$[\mathrm{Cl^\bullet}]_{ss} = \frac{k_{\mathrm{BA}} - k_{\mathrm{BA,\ HO^\bullet}}[\mathrm{HO^\bullet}]_{ss}}{k_{\mathrm{BA,\ Cl^\bullet}}} \tag{S10}$$

$$[\mathrm{ClO^\bullet}]_{ss} = \frac{k_{\mathrm{DMOB}} - k_{\mathrm{DMOB,\ HO^\bullet}}[\mathrm{HO^\bullet}]_{ss} - k_{\mathrm{DMOB,\ Cl^\bullet}}[\mathrm{Cl^\bullet}]_{ss}}{k_{\mathrm{DMOB,\ ClO^\bullet}}} \tag{S11}$$

$$[\mathrm{Cl_2^{\bullet-}}]_{ss} = \frac{k_{\mathrm{CBZ}} - k_{\mathrm{CBZ,\ HO^\bullet}}[\mathrm{HO^\bullet}]_{ss} - k_{\mathrm{CBZ,\ Cl^\bullet}}[\mathrm{Cl^\bullet}]_{ss} - k_{\mathrm{CBZ,\ ClO^\bullet}}[\mathrm{ClO^\bullet}]_{ss}}{k_{\mathrm{CBZ,\ Cl_2^{\bullet-}}}} \tag{S12}$$

Text S3. Calculation of Specific Energy Consumption (SEC). The SEC was calculated as the amount of electric energy needed to remove a certain weight of COD, according to the following equation (eq S13):

$$\mathrm{SEC} = \frac{U \times I \times t \times 10^{-3}}{V \times (C_0 - C_t) \times 10^{-6}} \tag{S13}$$

where U represents the average voltage measured during the electrolysis (V), I refers to the applied current (A), t is the electrolytic time (h), V is the volume of the experimental solution (0.3 L), and C_0 and C_t are the concentrations (mg L^{-1}) of COD at time 0 and time t, respectively.

Text S4. Calculation of Faradaic Efficiency (FE). The FE of anodic oxidation or cathodic reduction was defined as the ratio of the coulombs calculated from the measured amount of a substance removed (according to Faraday's law) to the coulombs actually applied to the electrode (eq S14).

$$\text{FE (\%)} = \frac{n_i \times F \times (C_0 - C_t) \times V}{I \times t} \times 100 \quad \text{(S14)}$$

where n_i represents the number of electrons required to oxidize or reduce substance I; F is the Faraday constant (96485.3 C mol^{-1}); C_0 and C_t are the concentrations (mol L^{-1}) of the substance i at the reaction times of 0 and t (s), respectively; V is the volume of the reactor (0.3 L); and I is the current (A). It should be noted that n equals 4 for COD oxidation expressed per mol of oxygen, 3 for ammonia oxidation to nitrogen gas, and 8 for nitrate reduction to ammonia. Ammonia is originated from nitrate reduction at the cathode, and its initial concentration is estimated based on the detected concentration in the electrochemical cell without the involvement of Cl^- (Figure S3c). This is because the presence of Cl^- in the solution does not alter the essential nature of nitrate reduction and the appropriate level of Cl^- has negligible impact on the ability of Cu/Zn cathode to reduce nitrate.[9,10]

Text S5. Toxicology Analysis. For enrichment, 5.0 mL of M9 medium, 10.25 mL of deionized water, 0.25 mL of mineral solution (see its composition in Table S2), 1 mL of glucose (20 g L^{-1}), 0.5 mL of *Escherichia coli* bacterial fluid, and 4 mL of sample wastewater were added into a 50 mL triangle bottle, which was orbitally shaken at 150 rpm (37 °C). After 24 h of culturing, the samples were collected and taken for immediate reactive oxygen species (ROS) and apoptosis analyses.

i) Analysis of intracellular ROS

The levels of ROS in cells were detected using 2,7-dichlorofluorescin diacetate (DCFH-DA) as an indicator. When DCFH-DA is absorbed by cells, the esterase in the cells results in its hydrolyzation into DCFH, and DCFH can be further oxidized by ROS to form fluorescent DCF. Then, the extent of ROS is characterized by measuring the fluorescence intensity. The microorganisms cultured for 24 h were collected and suspended in 10 μM DCFH-DA water solution to adjust the cell concentration of 10^6-10^7 mL^{-1}, followed by incubation in a cell incubator in the dark at 37 °C for 20 min. Subsequently, a flow cytometer was applied to measure the intensity of ROS.

ii) Analysis of apoptosis

Annexin V-PI is a widely used method for apoptosis analyses owing to its ability to distinguish cells in different apoptotic stages. Annexin V is one of the most effective indicators for detecting early cell apoptosis, and it has a good affinity with phosphatidylserine (PS). PS is only distributed inside the lipid bilayer of the cell membrane in normal cells in which Annexin V is not able to bind to PS. However, when the cells are in the early apoptosis stage, PS in the cell membrane turns from the inside to the outside. Then, fluorescently labeled Annexin V and PS are taken together, and we can distinguish normal cells from early apoptotic cells by detecting AV fluorescent signals. Propidium iodide (PI) is a nucleic acid dye that is not capable of

penetrating the intact cell membrane but can stain the nucleus of advanced and dead cells. We used Annexin V and PI together to differentiate cells at different stages of apoptosis. The Annexin V reagent and the PI dye solution were added to 1 mL of the cell suspension with a cell concentration of 10^6-10^7 mL^{-1} and incubated in the dark at room temperature for 5 min. Subsequently, we analyzed the apoptotic stages using a flow cytometer.

Text S6. Kinetic Modeling for Predicting Radical Concentrations. To predict the concentrations of radicals (i.e., $HO^{\bullet}$, $Cl^{\bullet}$, $Cl_2^{\bullet-}$, and $ClO^{\bullet}$) available in the electrochemical system when the electrolyte contains Cl^- and HCO_3^-, kinetic modeling was performed using Kintecus 6.80 software[11] (with a Bader-Deuflhard integrator) based on the 48 equations illustrated in Table S3. These include electrochemical reactions of $HO^{\bullet}$ and active chlorine (and its radical) generation, transformation reactions of reactive oxygen species, transformation reactions of chlorine radicals ($Cl^{\bullet}$, $Cl_2^{\bullet-}$, and $ClO^{\bullet}$), reactions of HCO_3^-/CO_3^{2-}-mediated $ClO^{\bullet}$ generation, and quenching reactions of radicals by carbamazepine (CBZ). The radical concentrations were modeled and plotted against time (duration of 60 min).

As presented in Figure S5a, the predicted concentration of $ClO^{\bullet}$ as a consequence of a series of transformation reactions in the electrochemical system with Cl^- and HCO_3^- was 1.22×10^{-12} M, which was around one to three orders of magnitude higher than those of $Cl_2^{\bullet-}$ (5.41×10^{-14} M), $Cl^{\bullet}$ (5.02×10^{-16} M), and $HO^{\bullet}$ (1.85×10^{-15} M). Taking into account the concentrations of these free radicals and their reaction rate constants with CBZ, the relative contributions of different free radicals to CBZ degradation were calculated from the model (Figure S5b). It is apparent that $ClO^{\bullet}$ is the main contributor to the disappearance of CBZ. We further ran the kinetic modeling by individually considering the contribution of eqs R37−R44 to $ClO^{\bullet}$ formation and ignoring the contribution of eqs R29−R32. In this case (Figure S6), the simulated concentration of $ClO^{\bullet}$ with 10 mM HCO_3^- was 2.25×10^{-13} M, whereas no $ClO^{\bullet}$ was derived without HCO_3^- (1×10^{-55} M is the minimum value of the simulation). This remarkable difference verifies that HCO_3^- plays a predominant role in mediating the production of $ClO^{\bullet}$.

Text S7. Generation of Active Chlorine and Chlorate during Wastewater Electrolysis. The concentrations of active chlorine and chlorate during wastewater electrolysis under varying current densities were measured. Note that active chlorine is a collective term for the sum of free chlorines included Cl_2, HClO, and ClO^-, which was determined by the N,N-diethyl-p-phenylenediamine (DPD) method as previously described.[5,12] It is evident in Figure S2 that the increasing current density yielded increases in both active chlorine and chlorate concentrations. Close observation reveals that the yield rates of active chlorine and chlorate during the first 3 h of operation were much smaller than in the last 3 h of operation. The lower yields were closely linked to the rapid removal of COD and TN (Figure 1) observed in the first 3 h of operation. This result is reasonable because, in the first period, most of the active chlorine is engaged in the generation of chlorine radicals that account for COD and ammonia oxidation, and, in the second period, the shortage of COD and ammonia causes the accumulation of active chlorine and chlorate, in accordance with the finding previously reported.[13,14] In addition, higher current densities such as 50 mA cm^{-2} led to an enhanced rate of chlorate formation, which resulted from the overoxidation of active chlorine. This explains the slow rise in the reaction rate of COD removal from 37.5 mA cm^{-2} to 50 mA cm^{-2}.

Text S8. Procedures for Changing Concentrations of HCO_3^- and Cl^- in Wastewater. Since carbonic acid is a weak acid, it can escape from the solution in the form of CO_2 under conditions of pH ≤ 4. To remove HCO_3^- (initial concentration of 10 mM) from the raw wastewater, the wastewater sample was heated to 35 ºC at 300 rpm, followed by pH adjustment by adding 1 M H_2SO_4. After 30 min of stirring, the pH value was readjusted to the original value. Through this process, HCO_3^--free wastewater was obtained. An appropriate amount of $NaHCO_3$ powder was added to the raw wastewater to obtain one wastewater sample containing 20 mM HCO_3^- and another wastewater sample containing 40 mM HCO_3^-.

Because of the much lower k_{sp} of AgCl (1.8×10^{-10}) compared with Ag_2SO_4 (1.4×10^{-5}), Ag_2SO_4 was added to the wastewater to remove Cl^- (initial concentration of 40 mM) from the wastewater by precipitation. Ag_2SO_4 powder in a molar ratio of Cl^-: Ag^+ = 1: 1 was slowly injected into the HCO_3^--free wastewater, which was stirred for 30 min at 300 rpm. After 30 min, the wastewater was centrifuged for 5 min at 8000 rpm, and the precipitates were removed from the solution. In this way, the Cl^--free wastewater sample was obtained. An appropriate amount of NaCl powder was amended to the Cl^--free wastewater to obtain a wastewater sample containing 20 mM Cl^- and to the raw wastewater to obtain a wastewater sample containing 60 mM Cl^-. The Cl^--free samples not containing HCO_3^- were replenished with $NaHCO_3$ powder to assure that the HCO_3^- concentration was identical to that (10 mM) in the raw wastewater.

Text S9. Evidence of Insignificant Role of Direct Anodic Oxidation. To discern the contribution of direct anodic oxidation to the removal of COD, linear sweep voltammetry (LSV) tests were conducted in the real wastewater versus synthetic wastewater. (The conductivity was controlled at the same value for both cases by adding Na_2SO_4 solution.) Figure S10 illustrates that slightly higher anodic currents were generated from the real wastewater, indicating that a small portion of organics available in secondary coking wastewater effluent can be directly oxidized at the anode. Nevertheless, whether they can be completely mineralized remains unknown. Further control experiments were performed by adding excessive HCO_3^- (500 mM) to the electrochemical system, which is thought to quench all the radicals and reactive chlorine.[5] Figure S11 clearly illustrates that the concentration of COD did not drop after 6 h of operation, suggesting the insignificant role of direct anodic oxidation.

Text S10. Comparison of Substrate-Specific Oxidizing Capacity between Chlorine Radicals (i.e., $ClO^{\bullet}$, $Cl_2^{\bullet-}$, and $Cl^{\bullet}$) and $HO^{\bullet}$. To support the conclusion that chlorine radicals (i.e., $ClO^{\bullet}$, $Cl_2^{\bullet-}$, and $Cl^{\bullet}$) are more selective oxidants and exhibit superior substrate-specific oxidizing capacity than $HO^{\bullet}$, two series of electrochemical oxidation experiments were performed and compared in electrolytes of Na_2SO_4 and NaCl. For the experimental conditions we adopted, it was considered that the $HO^{\bullet}$ electrogenerated from the discharge of water is the main oxidative species for pollutant degradation in the case of Na_2SO_4 and that the chlorine radicals resulting from Cl^- oxidation are the main contributors to the oxidation of pollutants in the case of NaCl, as demonstrated in the previous reports.[5,15] Phenolic compounds differing in their substituents were selected as the target contaminants to study the structure-specific activity because they are frequently detected compounds in coking wastewater[16] and their oxidation proceeds via similar reaction pathways.[17-19] The Hammett constants that quantitatively represent the electron-donating ability of the substituent[20] were used as the descriptors and are listed in Table S4.

Figure S12 depicts and compares the variations in the percentages of pollutant removal as a function of electrolysis time in the presence of Na_2SO_4 and NaCl. To rule out the possible contribution of $HO^{\bullet}$, NB was added to quench it in the electrolyte of NaCl. It was clear that the presence of NaCl significantly promoted the degradation of phenols. The apparent first-order rate constants were calculated and plotted against the Hammett constants (Figure S13). The $HO^{\bullet}$-mediated oxidation of phenols was not relevant to the Hammett constants. Conversely, the phenol degradation mediated by chlorine radicals was highly sensitive to the Hammett constants. A linear correlation between the rate constant and the Hammett constant is exhibited, with the electron-rich compounds delivering high reaction kinetics. These results verify that

chlorine radicals are more selective oxidants than $HO^{\bullet}$ and preferentially react with electron-rich compounds.

Table S1. Main water quality parameters of secondary coking wastewater effluent.

Constituent	Value
pH	7.9 ± 0.2
COD (mg L^{-1})	228.1 ± 8.6
TOC (mg L^{-1})	62.2 ± 2.2
Conductivity (mS cm^{-1})	12.5 ± 0.3
Cl^- (mg L^{-1})	1422.1 ± 12.6
SO_4^{2-} (mg L^{-1})	2333.9 ± 18.4
HCO_3^- (mg L^{-1})	619.4 ± 8.5
NO_3^--N (mg L^{-1})	76.2 ± 2.3
TN (mg L^{-1})	79.8 ± 3.1
Hydrophilic composition	72.23%
Hydrophobic composition	26.48%
UV_{254} (cm^{-1})	2.34
$SUVA_{254}$ (L mg^{-1} m^{-1})	3.78

Table S2. Components of mineral solution used for microbial culture.

Constituent	Concentration (g L^{-1})
$N(CH_2COOH)_3$	1.5
H_3BO_3	0.01
NaCl	1.0
$CaCl_2$	1.0
$MnSO_4 \cdot H_2O$	0.5
$Na_2MoO_4 \cdot 2H_2O$	0.01
$CuSO_4 \cdot 5H_2O$	0.01
$CoCl_2 \cdot 6H_2O$	0.1
$MgSO_4 \cdot 7H_2O$	3.0
$FeSO_4 \cdot 7H_2O$	0.1
$ZnSO_4 \cdot 7H_2O$	0.1
$AlK(SO_4)_2 \cdot 12H_2O$	0.01

Table S3. Key reactions involved in the generation of radicals in the electrochemical system in the presence of Cl^- and HCO_3^-.

No.	Reaction	Rate constant	Reference
	Electrochemical reactions		
R1	$H_2O \rightarrow HO^\bullet + H^+ + e^-$	$7.92 \times 10^{-9}\ s^{-1}$	
R2	$Cl^- \rightarrow Cl^\bullet + e^-$	$1.49 \times 10^{-9}\ s^{-1}$	
R3	$2\ Cl^- \rightarrow Cl_2$	$1.45 \times 10^{-2}\ s^{-1}$	
	pH-dependent equilibrium reactions		
R4	$H^+ + OH^- \rightarrow H_2O$	$1 \times 10^{11}\ M^{-1}\ s^{-1}$	21
R5	$H_2O \rightarrow H^+ + OH^-$	$1 \times 10^{-3}\ s^{-1}$	21
R6	$OCl^- + H^+ \rightarrow HOCl$	$5 \times 10^{10}\ M^{-1}\ s^{-1}$	21
R7	$HOCl \rightarrow OCl^- + H^+$	$1.6 \times 10^{3}\ s^{-1}$	21
R8	$Cl_2 + H_2O \rightarrow Cl_2OH^- + H^+$	$1.5 \times 10^{1}\ M^{-1}\ s^{-1}$	22
R9	$Cl^- + HOCl \rightarrow Cl_2OH^-$	$1.5 \times 10^{4}\ M^{-1}\ s^{-1}$	22
R10	$Cl_2OH^- \rightarrow Cl^- + HOCl$	$5.5 \times 10^{-11}\ s^{-1}$	22
R11	$HCO_3^- \rightarrow H^+ + CO_3^{2-}$	$5.61 \times 10^{9}\ s^{-1}$	8
R12	$H^+ + CO_3^{2-} \rightarrow HCO_3^-$	$5 \times 10^{10}\ M^{-1}\ s^{-1}$	8
	Reactive oxygen species transformation reactions		
R13	$HO^\bullet + HO^\bullet \rightarrow H_2O_2$	$5.5 \times 10^{9}\ M^{-1}\ s^{-1}$	3
R14	$HO^\bullet \rightarrow O^{\bullet-} + H^+$	$1.26 \times 10^{12}\ s^{-1}$	3
R15	$O^{\bullet-} + H_2O \rightarrow HO^\bullet + OH^-$	$1.8 \times 10^{6}\ M^{-1}\ s^{-1}$	3
R16	$HO^\bullet + OH^- \rightarrow O^{\bullet-} + H_2O$	$1.3 \times 10^{10}\ M^{-1}\ s^{-1}$	3
	Reactive chlorine species transformation reactions		
R17	$Cl^- + HO^\bullet \rightarrow ClOH^{\bullet-}$	$4.3 \times 10^{9}\ M^{-1}\ s^{-1}$	3
R18	$ClOH^{\bullet-} \rightarrow Cl^- + HO^\bullet$	$6.1 \times 10^{9}\ s^{-1}$	23
R19	$Cl^\bullet + OH^- \rightarrow ClOH^{\bullet-}$	$1.8 \times 10^{10}\ M^{-1}\ s^{-1}$	24
R20	$ClOH^{\bullet-} + H^+ \rightarrow Cl^\bullet + H_2O$	$2.1 \times 10^{10}\ M^{-1}\ s^{-1}$	25
R21	$ClOH^{\bullet-} + Cl^- \rightarrow Cl_2^{\bullet-} + OH^-$	$1 \times 10^{5}\ M^{-1}\ s^{-1}$	25
R22	$Cl_2^{\bullet-} + OH^- \rightarrow ClOH^{\bullet-} + Cl^-$	$4.5 \times 10^{7}\ M^{-1}\ s^{-1}$	25
R23	$Cl^\bullet + Cl^- \rightarrow Cl_2^{\bullet-}$	$6.5 \times 10^{9}\ M^{-1}\ s^{-1}$	24
R24	$Cl_2^{\bullet-} \rightarrow Cl^\bullet + Cl^-$	$1.1 \times 10^{5}\ s^{-1}$	23
R25	$Cl^\bullet + Cl^\bullet \rightarrow Cl_2$	$1 \times 10^{8}\ M^{-1}\ s^{-1}$	15
R26	$Cl^\bullet + Cl_2^{\bullet-} \rightarrow Cl_2 + Cl^-$	$1.4 \times 10^{9}\ M^{-1}\ s^{-1}$	26
R27	$Cl_2^{\bullet-} + Cl_2^{\bullet-} \rightarrow Cl_2 + 2Cl^-$	$8.3 \times 10^{8}\ M^{-1}\ s^{-1}$	23
R28	$Cl_2^{\bullet-} + HO^\bullet \rightarrow HOCl + Cl^-$	$1 \times 10^{9}\ M^{-1}\ s^{-1}$	23
R29	$HO^\bullet + HOCl \rightarrow ClO^\bullet + H_2O$	$2 \times 10^{9}\ M^{-1}\ s^{-1}$	21

R30	$HO^{\bullet} + OCl^{-} \rightarrow ClO^{\bullet} + OH^{-}$	8.8×10^{9} M^{-1} s^{-1}	27
R31	$Cl^{\bullet} + HOCl \rightarrow ClO^{\bullet} + Cl^{-} + H^{+}$	3×10^{9} M^{-1} s^{-1}	15
R32	$Cl^{\bullet} + OCl^{-} \rightarrow ClO^{\bullet} + Cl^{-}$	8.2×10^{9} M^{-1} s^{-1}	23
R33	$ClO^{\bullet} + ClO^{\bullet} \rightarrow Cl_2O_2$	2.5×10^{9} M^{-1} s^{-1}	8
R34	$2ClO^{\bullet} + H_2O \rightarrow HOCl + H^{+} + ClO_2^{-}$	2.5×10^{9} M^{-1} s^{-1}	8
R35	$2ClO^{\bullet} + OH^{-} \rightarrow OCl^{-} + H^{+} + ClO_2^{-}$	2.5×10^{9} M^{-1} s^{-1}	8
R36	$ClO^{\bullet} + HO^{\bullet} \rightarrow H^{+} + ClO_2^{-}$	1×10^{9} M^{-1} s^{-1}	8
	HCO_3^{-}/CO_3^{2-}-mediated $ClO^{\bullet}$ generation reactions		
R37	$HO^{\bullet} + HCO_3^{-} \rightarrow CO_3^{\bullet-} + H_2O$	8.5×10^{6} M^{-1} s^{-1}	25
R38	$HO^{\bullet} + CO_3^{2-} \rightarrow CO_3^{\bullet-} + OH^{-}$	3.9×10^{8} M^{-1} s^{-1}	25
R39	$Cl^{\bullet} + HCO_3^{-} \rightarrow CO_3^{\bullet-} + Cl^{-} + H^{+}$	2.2×10^{8} M^{-1} s^{-1}	25
R40	$Cl^{\bullet} + CO_3^{2-} \rightarrow CO_3^{\bullet-} + Cl^{-}$	5×10^{8} M^{-1} s^{-1}	25
R41	$Cl_2^{\bullet-} + HCO_3^{-} \rightarrow CO_3^{\bullet-} + 2Cl^{-} + H^{+}$	8×10^{7} M^{-1} s^{-1}	25
R42	$Cl_2^{\bullet-} + CO_3^{2-} \rightarrow CO_3^{\bullet-} + 2Cl^{-}$	1.6×10^{8} M^{-1} s^{-1}	25
R43	$CO_3^{\bullet-} + OCl^{-} \rightarrow ClO^{\bullet} + CO_3^{2-}$	5.7×10^{5} M^{-1} s^{-1}	25
R44	$ClO^{\bullet} + CO_3^{2-} \rightarrow CO_3^{\bullet-} + OCl^{-}$	6×10^{2} M^{-1} s^{-1}	25
	Radicals quenched by carbamazepine (CBZ)		
R45	$HO^{\bullet}$ + CBZ → product 1	8.8×10^{9} M^{-1} s^{-1}	7
R46	$Cl^{\bullet}$ + CBZ → product 2	3.3×10^{10} M^{-1} s^{-1}	6
R47	$Cl_2^{\bullet-}$ + CBZ → product 3	4.3×10^{7} M^{-1} s^{-1}	6
R48	$ClO^{\bullet}$ + CBZ → product 4	1.97×10^{8} M^{-1} s^{-1}	8

Table S4. Hammett constants (σ) of different *p*-substituents, including *p*-aminophenol (*p*-NH_2), *p*-cresol (*p*-CH_3), phenol (*p*-H), 4-chlorophenol (*p*-Cl), and *p*-nitrophenol (*p*-NO_2).

Substituent	σ
p-NH_2	-0.66
p-CH_3	-0.17
p-H	0
p-Cl	0.23
p-NO_2	0.78

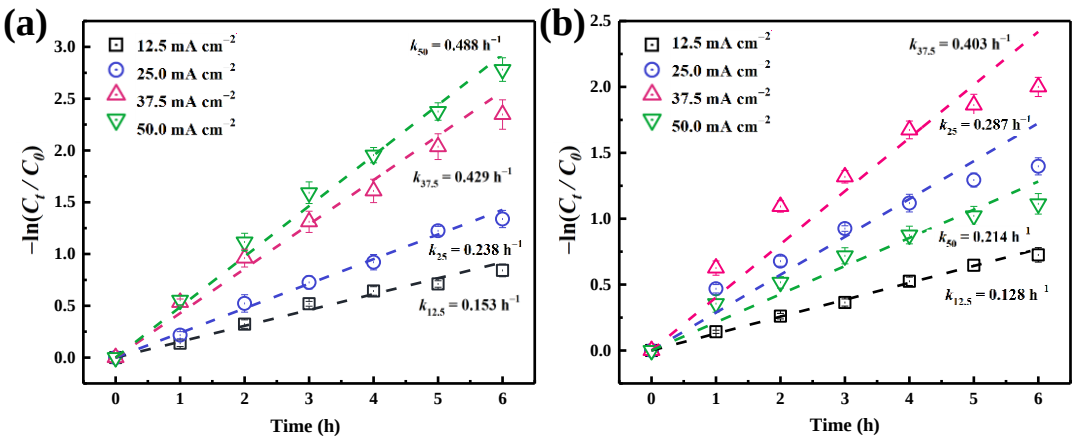

Figure S1. Plots of -ln(C_t/C_0) versus time for (a) COD and (b) TN removal at different current densities in the coupled electrochemical system.

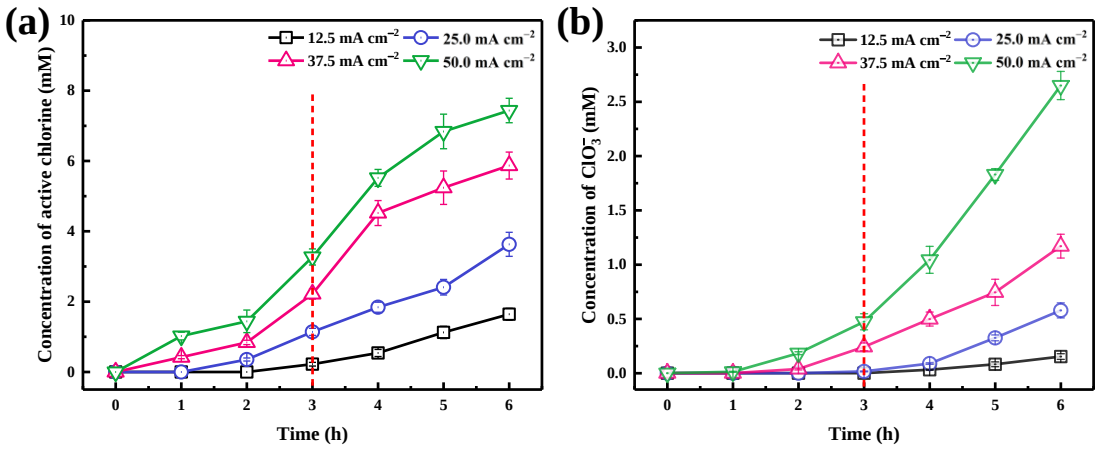

Figure S2. Variations in the concentrations of (a) active chlorine and (b) chlorate as a function of reaction time during wastewater electrolysis at different current densities.

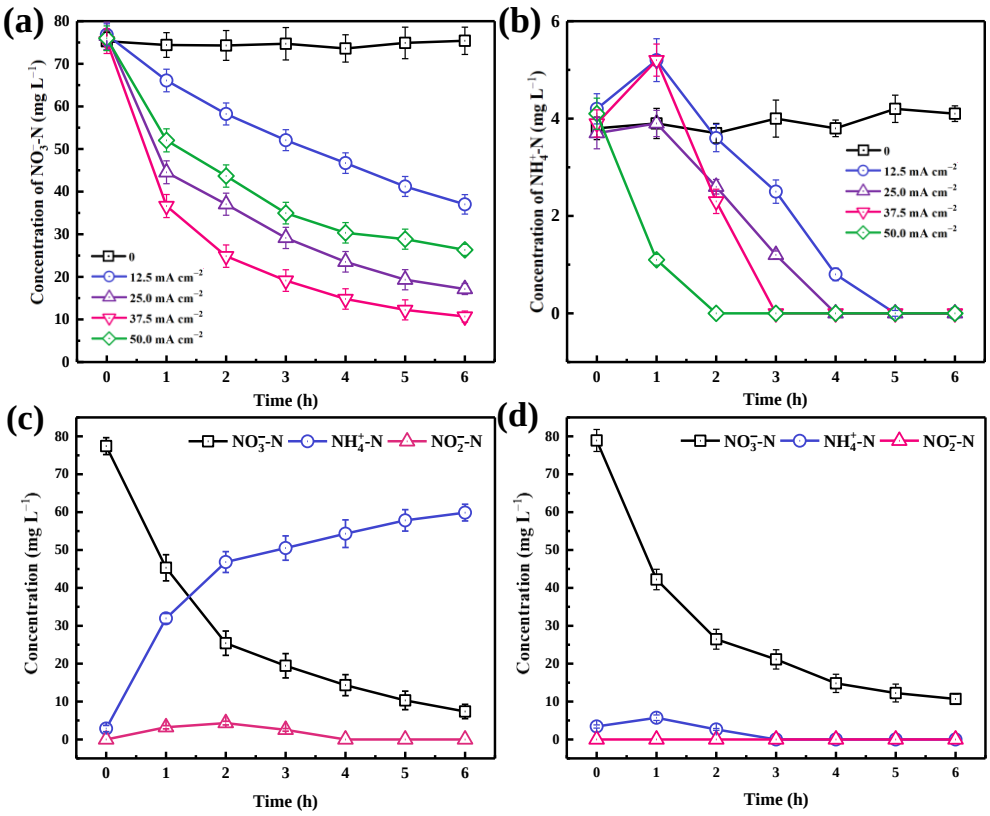

Figure S3. Time courses of (a) NO_3^--N and (b) NH_4^+-N concentrations in secondary coking wastewater effluent treated via the coupling electrochemical system: effect of current density. Time courses of NO_3^--N, NO_2^--N, and NH_4^+-N in synthetic wastewater treated via the coupling electrochemical system in the (c) absence and (d) presence of 40 mM NaCl.

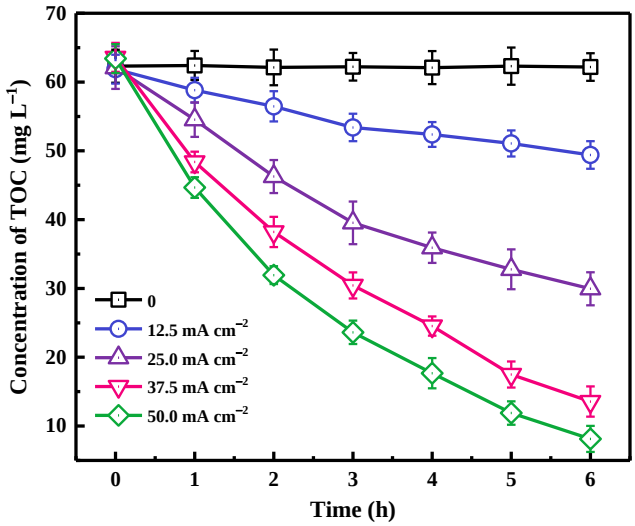

Figure S4. Time courses of total organic carbon (TOC) concentrations in secondary coking wastewater effluent treated via the coupled electrochemical system: effect of current density.

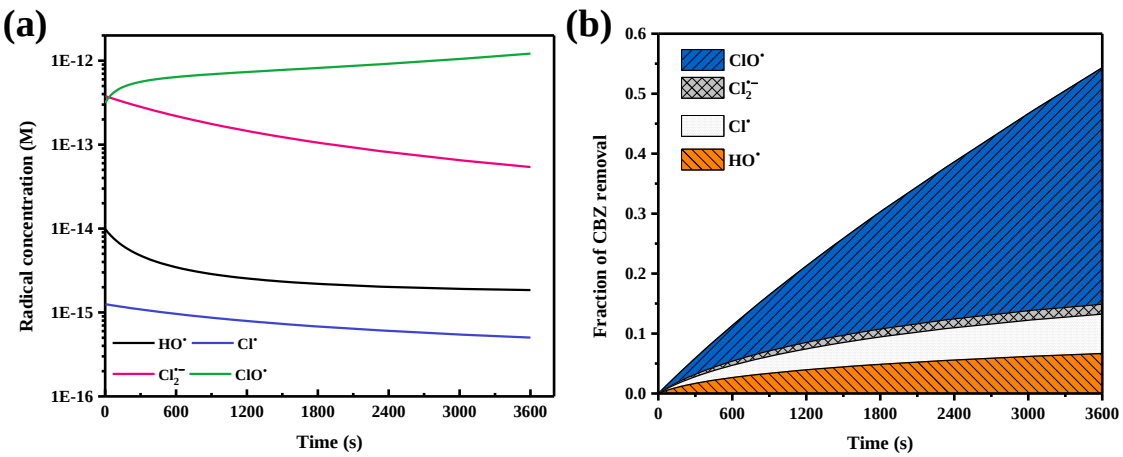

Figure S5. (a) Predicted concentrations of $HO^{\bullet}$, $Cl^{\bullet}$, $Cl_2^{\bullet-}$, and $ClO^{\bullet}$ in the electrochemical system containing Cl^- and HCO_3^-. (b) Fraction of carbamazepine (CBZ) removal contributed by $HO^{\bullet}$, $Cl^{\bullet}$, $Cl_2^{\bullet-}$, and $ClO^{\bullet}$. Experiment conditions: [CBZ] = 5 mM, $[Cl^-]$ = 40 mM, $[HCO_3^-]$ = 10 mM, reaction time = 60 min, and pH = 9.4.

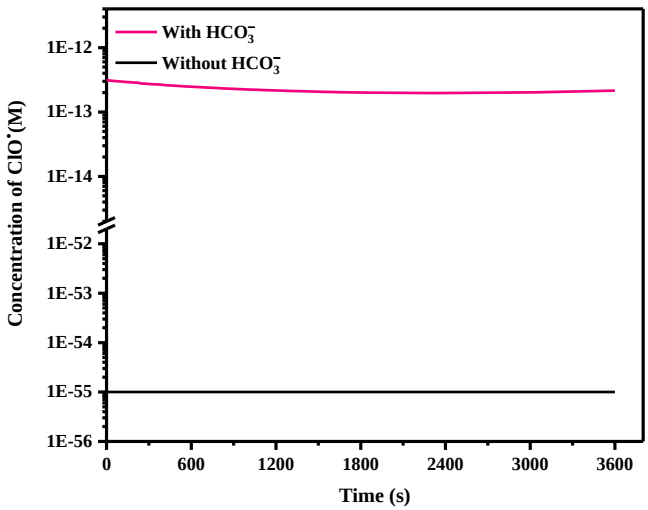

Figure S6. Predicted concentration of $ClO^{\bullet}$ in the presence and absence of HCO_3^- if the contribution of eqs. R29–R32 to $ClO^{\bullet}$ generation is ignored. Experiment conditions: [CBZ] = 5 mM, $[Cl^-]$ = 40 mM, $[HCO_3^-]$ = 10 mM, reaction time = 60 min, and pH = 9.4.

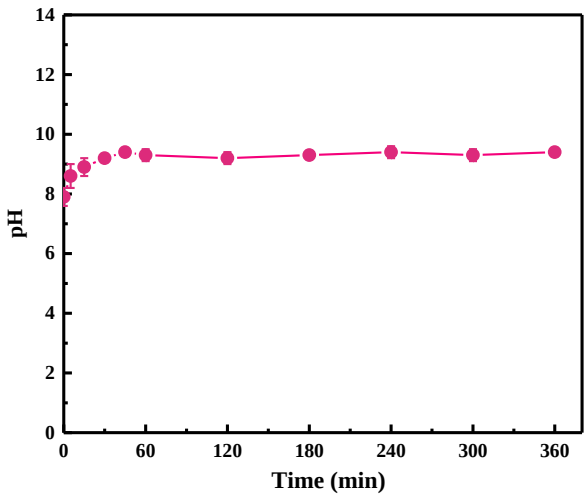

Figure S7. Variations in pH as a function of reaction time during wastewater electrolysis.

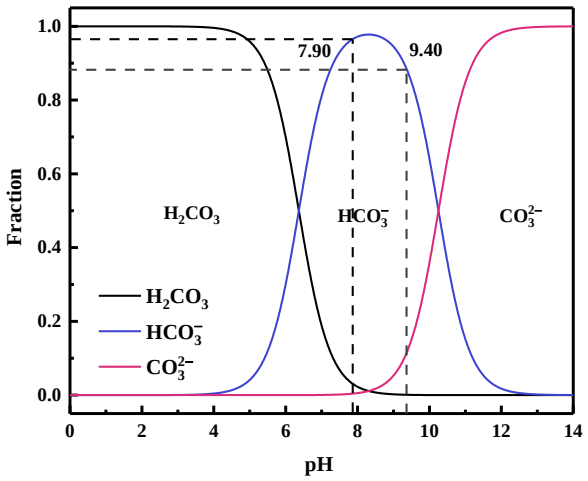

Figure S8. Theoretical fractions of carbonate species with respect to different pH levels at 25 ºC.

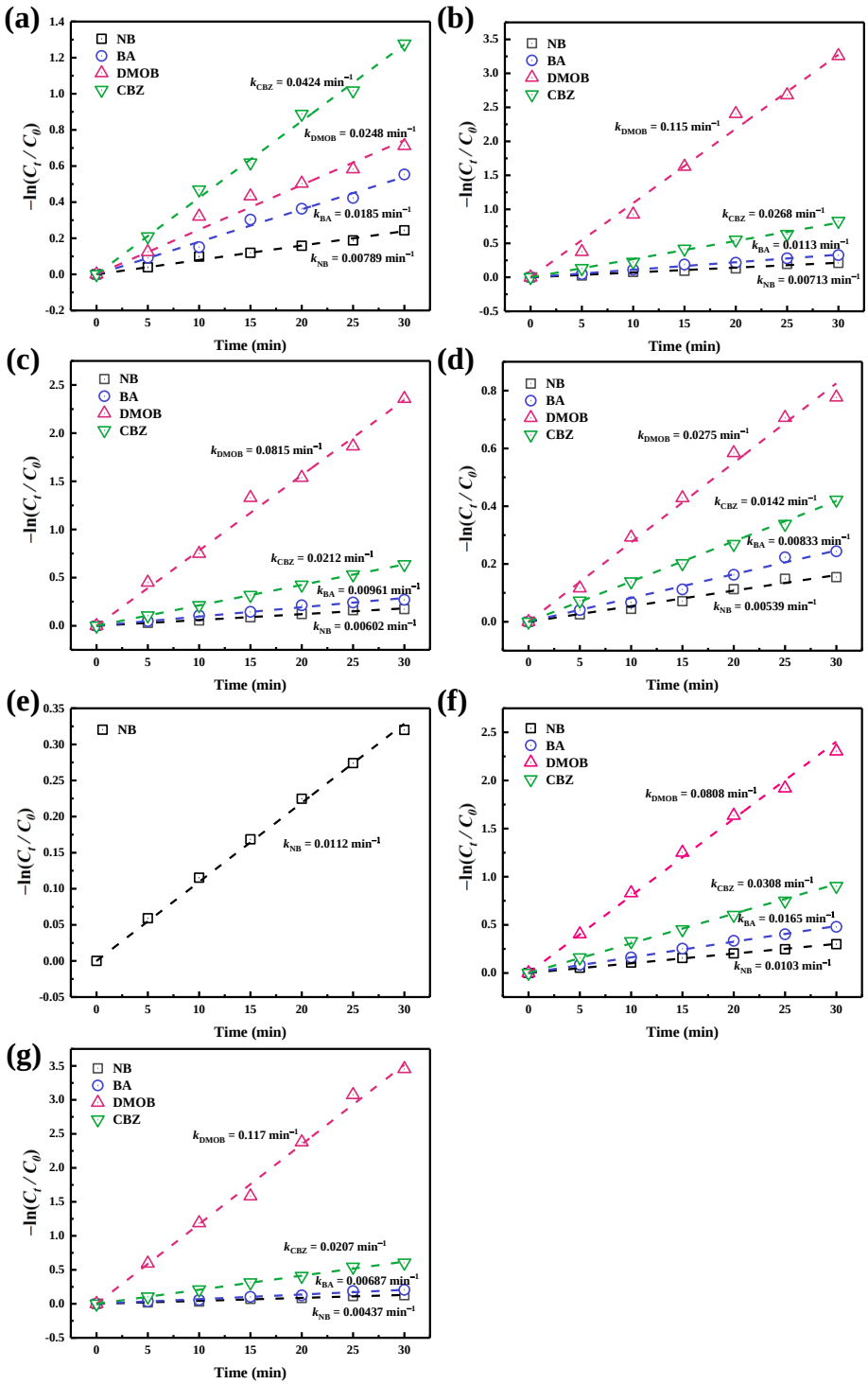

Figure S9. First-order decay of NB, BA, CBZ, and DMOB in the electrochemical system fed with real wastewater under different conditions. In (a-d), the concentration of Cl^- was kept at 40 mM and the concentration of HCO_3^- was varied at (a) 0, (b) 10 mM, (c) 20 mM, and (d) 40 mM. In (e-g), the concentration of HCO_3^- was kept at 10 mM, and the concentration of Cl^- was varied at (e) 0, (f) 20 mM, and (g) 60 mM.

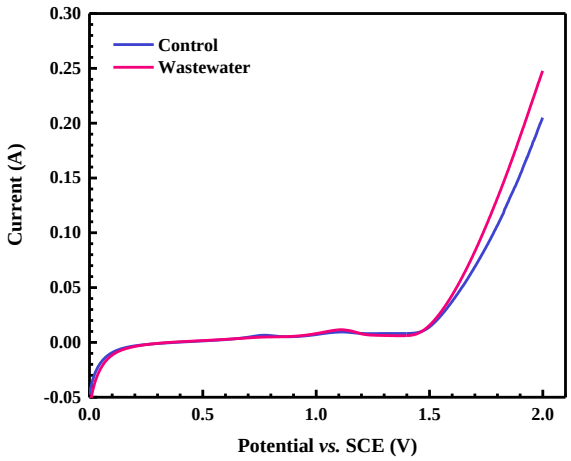

Figure S10. LSV curves of the PbO_2 anode recorded in secondary coking wastewater effluent and background electrolyte containing 40 mM Cl^-. Both solutions had the same conductivity, which was controlled by the addition of Na_2SO_4. Other experimental conditions: scan rate = 10 mV s^{-1} and initial pH = 7.9.

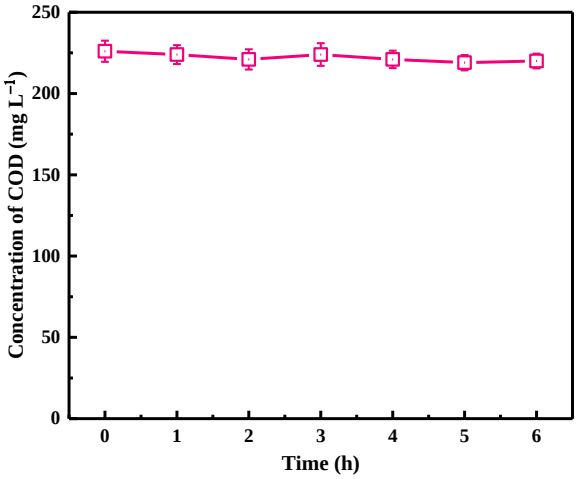

Figure S11. Time courses of COD concentrations in secondary coking wastewater effluent treated via the coupled electrochemical system. Experimental conditions: [HCO_3^-] = 500 mM, current density = 37.5 mA cm^{-2}, and initial pH = 7.9.

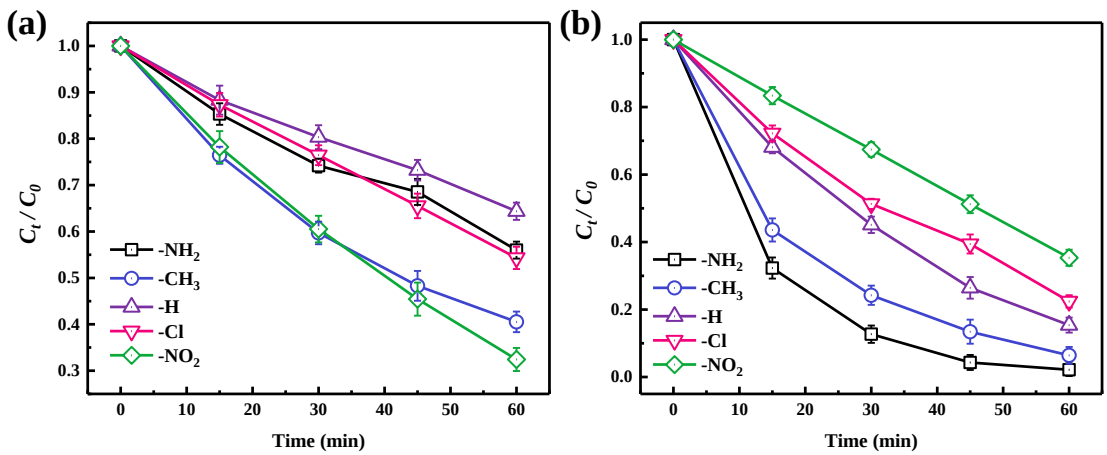

Figure S12. Anodic oxidation of *p*-substituted phenols in the electrochemical system with electrolytes of (a) Na_2SO_4 and (b) NaCl. Experiment conditions: [initial phenols] = 0.25 mM, reaction time = 60 min, current density = 37.5 mA cm^{-2}, and initial pH = 3.0. In (a), the concentration of Na_2SO_4 was 100 mM; in (b), the concentration of NaCl was 40 mM and the concentration of Na_2SO_4 (supporting electrolyte) was 80 mM.

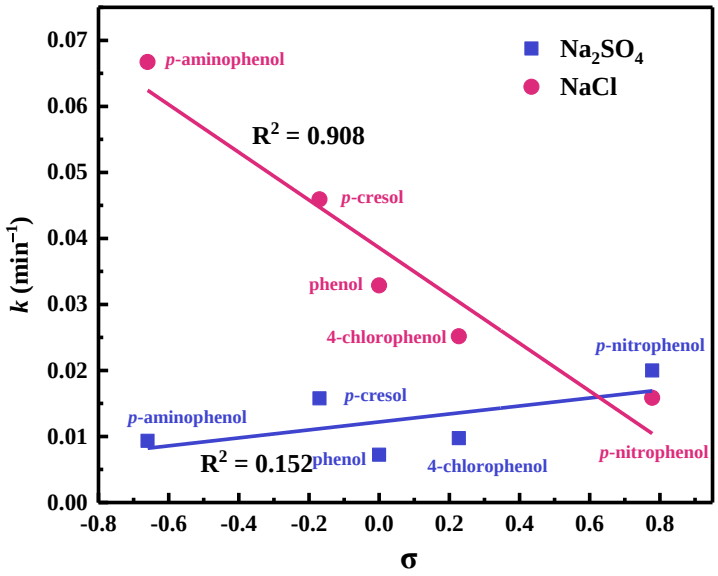

Figure S13. Correlations between the first-order reaction constant (*k*) of five *p*-substituted phenols obtained in Na_2SO_4 and NaCl solution and the Hammett constants (σ) of their *p*-substituents.

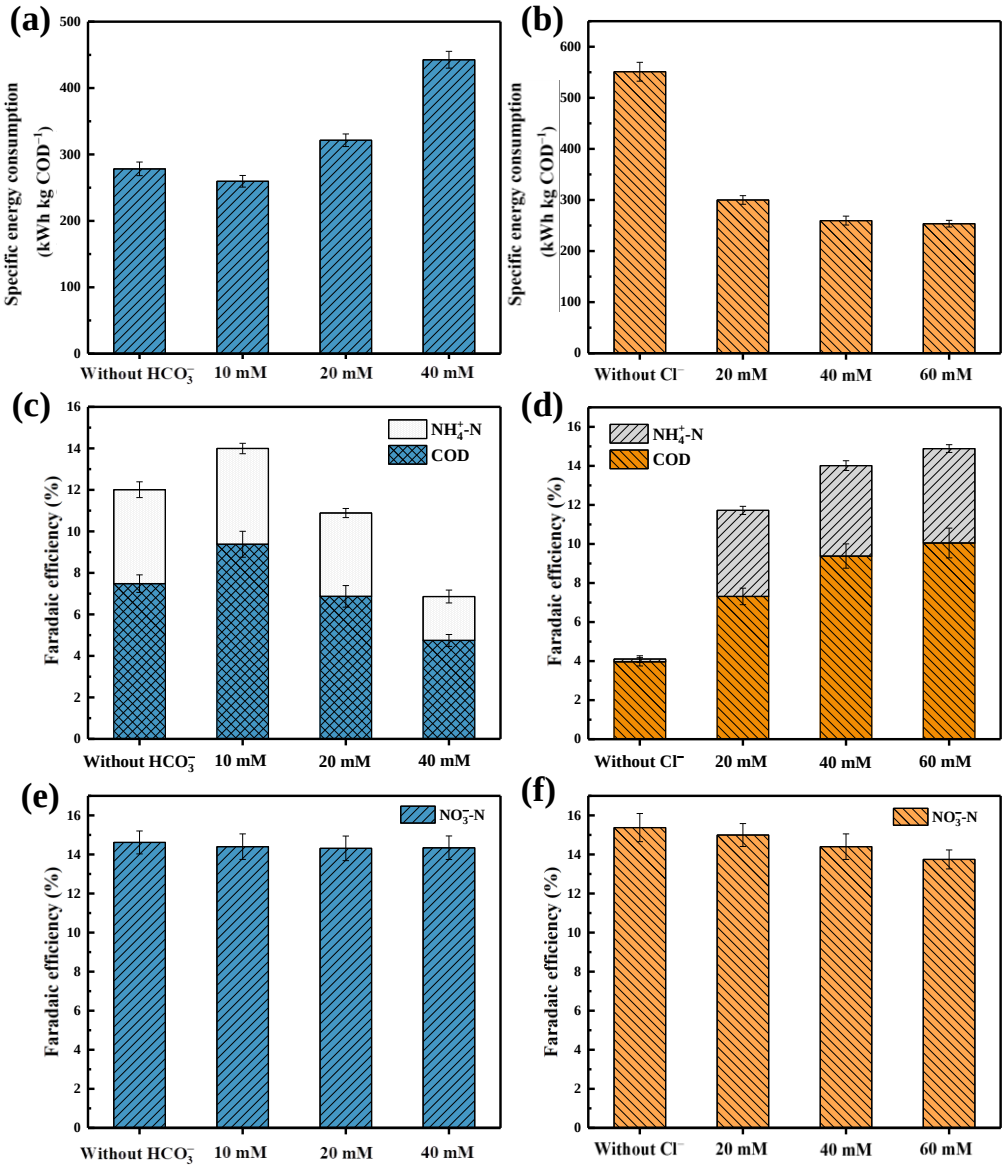

Figure S14. Calculated values of (a, b) SEC, (c, d) FE of anodic oxidation, and (e, f) FE of cathodic reduction as a function of concentrations of (a, c, e) HCO_3^- and (b, d, f) Cl^- after 3-h of wastewater electrolysis. In (a, c, e), the concentration of Cl^- was kept at 40 mM; in (b, d, f), the concentration of HCO_3^- was kept at 10 mM.

REFERENCES

(1) Fang, J.; Fu, Y.; Shang, C. The roles of reactive species in micropollutant degradation in the UV/free chlorine system. *Environ. Sci. Technol.* **2014,** *48* (3), 1859-1868.

(2) Alegre, M. L.; Geronés, M.; Rosso, J. A.; Bertolotti, S. G.; Braun, A. M.; Mártire, D. O.; Gonzalez, M. C. Kinetic study of the reactions of chlorine atoms and $Cl_2^{\bullet-}$ radical anions in aqueous solutions. 1. Reaction with benzene. *J.Phys. Chem. A* **2000,** *104* (14), 3117-3125.

(3) Buxton, G. V.; Greenstock, C. L.; Helman, W. P.; Ross, A. B. Critical review of rate constants for reactions of hydrated electrons, hydrogen atoms and hydroxyl radicals (·OH/·O−) in aqueous solution. *J. Phys. Chem. Ref. Data* **1988,** *17* (2), 513-886.

(4) Alfassi, Z. B.; Huie, R. E.; Mosseri, S.; Neta, P. Kinetics of one-electron oxidation by the ClO radical. *International Journal of Radiation Applications and Instrumentation. Part C. Radiation Physics and Chemistry* **1988,** *32* (1), 85-88.

(5) Zhang, Y.; Li, J.; Bai, J.; Li, L.; Chen, S.; Zhou, T.; Wang, J.; Xia, L.; Xu, Q.; Zhou, B. Extremely efficient decomposition of ammonia N to N_2 using $ClO^{\bullet}$ from reactions of $HO^{\bullet}$ and HOCl generated in situ on a novel bifacial photoelectroanode. *Environ. Sci. Technol.* **2019,** *53* (12), 6945-6953.

(6) Lei, Y.; Cheng, S.; Luo, N.; Yang, X.; An, T. Rate constants and mechanisms of the reactions of $Cl^{\bullet}$ and $Cl_2^{\bullet-}$ with trace organic contaminants. *Environ. Sci. Technol.* **2019,** *53* (19), 11170-11182.

(7) Lian, L.; Yao, B.; Hou, S.; Fang, J.; Yan, S.; Song, W. Kinetic study of hydroxyl and sulfate radical-mediated oxidation of pharmaceuticals in wastewater effluents. *Environ. Sci. Technol.* **2017,** *51* (5), 2954-2962.

(8) Guo, K.; Wu, Z.; Yan, S.; Yao, B.; Song, W.; Hua, Z.; Zhang, X.; Kong, X.; Li, X.; Fang, J. Comparison of the UV/chlorine and UV/H_2O_2 processes in the degradation of PPCPs in simulated drinking water and wastewater: kinetics, radical mechanism and energy requirements. *Water Res.* **2018,** *147*, 184-194.

(9) Li, M.; Feng, C.; Zhang, Z.; Lei, X.; Chen, R.; Yang, Y.; Sugiura, N. Simultaneous reduction of nitrate and oxidation of by-products using electrochemical method. *J. Hazard. Mater.* **2009,** *171* (1), 724-730.

(10) Fan, N.; Li, Z.; Zhao, L.; Wu, N.; Zhou, T. Electrochemical denitrification and kinetics study using Ti/IrO_2–TiO_2–RuO_2 as the anode and Cu/Zn as the cathode. *Chem. Eng. J.* **2013,** *214*, 83-90.

(11) Ianni, J. C. - A comparison of the bader-deuflhard and the cash-karp runge-kutta integrators for the GRI-MECH 3.0 model based on the chemical kinetics code kintecus. In *Computational Fluid and Solid Mechanics 2003*, Bathe, K. J., Ed. Elsevier Science Ltd: Oxford, **2003,** 1368-1372.

(12) Cho, K.; Hoffmann, M. R. $Bi_xTi_{1-x}O_z$ functionalized heterojunction anode with an enhanced reactive chlorine generation efficiency in dilute aqueous solutions. *Chem. Mater.* **2015,** *27* (6), 2224-2233.

(13) Jasper, J. T.; Yang, Y.; Hoffmann, M. R. Toxic byproduct formation during

electrochemical treatment of latrine wastewater. *Environ. Sci. Technol.* **2017,** *51* (12), 7111-7119.
(14) Cho, K.; Qu, Y.; Kwon, D.; Zhang, H.; Cid, C. A.; Aryanfar, A.; Hoffmann, M. R. Effects of anodic potential and chloride ion on overall reactivity in electrochemical reactors designed for solar-powered wastewater treatment. *Environ. Sci. Technol.* **2014,** *48* (4), 2377-2384.
(15) Yang, Y.; Shin, J.; Jasper, J. T.; Hoffmann, M. R. Multilayer heterojunction anodes for saline wastewater treatment: design strategies and reactive species generation mechanisms. *Environ. Sci. Technol.* **2016,** *50* (16), 8780-8787.
(16) Zhu, X.; Ni, J.; Lai, P. Advanced treatment of biologically pretreated coking wastewater by electrochemical oxidation using boron-doped diamond electrodes. *Water Res.* **2009,** *43* (17), 4347-4355.
(17) Bhosale, G. S.; Vaidya, P. D.; Joshi, J. B.; Patil, R. N. Kinetics of ozonation of phenol and substituted phenols. *Ind. & Eng. Chem. Res.* **2019,** *58* (18), 7461-7466.
(18) Martino, C. J.; Savage, P. E. Supercritical water oxidation kinetics, products, and pathways for CH_3- and CHO-substituted phenols. *Ind. & Eng. Chem. Res.* **1997,** *36* (5), 1391-1400.
(19) Martino, C. J.; Savage, P. E. Supercritical water oxidation kinetics and pathways for ethylphenols, hydroxyacetophenones, and other monosubstituted phenols. *Ind. & Eng. Chem. Res.* **1999,** *38* (5), 1775-1783.
(20) Hansch, C.; Leo, A.; Taft, R. W. A survey of hammett substituent constants and resonance and field parameters. *Chem. Rev.* **1991,** *91* (2), 165-195.
(21) Martinez-Huitle, C. A.; Ferro, S. Electrochemical oxidation of organic pollutants for the wastewater treatment: direct and indirect processes. *Chem. Soc. Rev.* **2006,** *35* (12), 1324-1340.
(22) Wang, T. X.; Margerum, D. W. Kinetics of reversible chlorine hydrolysis: temperature dependence and general-acid/base-assisted mechanisms. *Inorg. Chem.* **1994,** *33* (6), 1050-1055.
(23) Jayson, G. G.; Parsons, B. J.; Swallow, A. J. Some simple, highly reactive, inorganic chlorine derivatives in aqueous solution. Their formation using pulses of radiation and their role in the mechanism of the fricke dosimeter. *Journal of the Chemical Society, Faraday Transactions 1: Physical Chemistry in Condensed Phases* **1973,** *69* (0), 1597-1607.
(24) Kläning, U. K.; Wolff, T. Laser flash photolysis of HClO, ClO^-, HBrO, and BrO^- in aqueous solution. reactions of Cl- and Br-atoms. *Berichte der Bunsengesellschaft für physikalische Chemie* **1985,** *89* (3), 243-245.
(25) Grebel, J. E.; Pignatello, J. J.; Mitch, W. A. Effect of halide ions and carbonates on organic contaminant degradation by hydroxyl radical-based advanced oxidation processes in saline waters. *Environ. Sci. Technol.* **2010,** *44* (17), 6822-6828.
(26) Park, H.; Vecitis, C. D.; Hoffmann, M. R. Electrochemical water splitting coupled with organic compound oxidation: the role of active chlorine species. *J. Phys. Chem. C.* **2009,** *113* (18), 7935-7945.
(27) Connick, R. E. The interaction of hydrogen peroxide and hypochlorous acid in

acidic solutions containing chloride ion. *J. Am. Chem. Soc.* **1947,** *69* (6), 1509-1514.